The Nucleus, **41** (1-4) 2004 : 1-6

**The Nucleus**
A Quarterly Scientific Journal of
Pakistan Atomic Energy Commission
NCLEAM, ISSN 0029-5698

# ION-INDUCED ELECTRON EMISSION FROM THE CARBON TARGETS

A. QAYYUM*, M.I. MAHMOOD[1] and W. AHMAD

Physics Research Division, PINSTECH, P.O. Nilore, Islamabad, Pakistan

[1]Electronics Division, PINSTECH, P.O. Nilore, Islamabad, Pakistan

(Received February 9, 2005 and accepted in revised form June 13, 2005)

We describe characteristics and operation of a secondary electron detector geometry, which is recently developed for measuring the ion-induced total electron emission yield, $\gamma$, and kinetic energy distribution of electrons released from solid targets. This setup has been successfully applied to measure $\gamma$ of a carbon target bombarded with 1-10 keV singly charged ions $Ne^+$ and $Ar^+$. It was observed that in investigated energy range $\gamma$ increases with the ion energy and mass. Moreover, the expected proportionality between $\gamma$ and electronic stopping power was found. The detector geometry is relatively simple and is suitable for measurements over wide range of ion energies and target materials. *PACS:* 34.50.Dy; 79.20. Rf

**Keywords**: Ion-induced electron emission; Carbon surface; Electronic stopping power

## 1. Introduction

Electron emission from solid surfaces by impact of fast projectile ions is one of the most fundamental processes in ion-solid interactions and has received a great deal of attention in the past decades [1-2]. This phenomenon, known as Ion-induced Electron Emission (IEE), is usually characterized by a coefficient $\gamma$ defined as the number of electrons ejected per incident ion. The IEE from metal surface is commonly ascribed to two different mechanisms, the potential emission [3] and the kinetic emission processes [4]. In potential emission electrons can be librated from the target by the energy released upon neutralization of the incident ion. This process can occur if the ground-state recombination energy of the ion exceeds twice the work function of the target and it has no kinetic energy threshold. The experimental studies on slow multicharged ion bombardment of metals have established a linear relationship between potential electron yield $\gamma_{PE}$ and the total ionization potential of respective bombarding ion [5]. Ions with velocities exceeding a certain threshold, typically $10^5$ $ms^{-1}$, can liberate electrons by kinetic emission. Here, the energy required to release electrons from the target is provided by the kinetic energy of the projectile. According to the most common theoretical models [6-7] the kinetic electron emission yield $\gamma_{KE}$ should be proportional to the energy loss of the ion near the target surface but significant deviation has been reported [8]. In general, although total secondary electron emission yield is given by the sum of these processes, the kinetic electron emission yields are dominant except for those at extremely low energy and highly charged ions. For comprehensive information on IEE, see reviews by Rosler and Brauer [9] and Hasselkamp [10].

The study of electron emission provides some of the most detailed pictures of inelastic ion-surface collisions that can be applied to study other processes, such as energy loss, charge transfer, ionization damage and desorption. These mechanisms can de described conceptually but calculations are still far from the level of accuracy. In addition, of being of fundamental importance, IEE studies are also relevant to technological applications encompassing such diverse fields as (i) secondary ion mass spectrometry, (ii) plasma-based processing technology, (iii) particle detector fabrication industry, (iv) preparation of new electronic materials using ion implantation, including the fabrication of Very large-Scale Integrated circuits (VLSI) and, quite importantly (v) plasma-wall interactions in electrical discharges and fusion plasmas [11, 12]. The use of low-Z materials such as carbon, boron and beryllium has proven beneficial in present-day large tokamaks

* Corresponding author: qayyum@pinstech.org.pk

[13]. In ITER design, graphite-based low-Z material is recommended for divertor plates and first wall protection, in order to minimize the risks of plasma contamination. Available databases on plasma-surface interaction (PSI) mainly include physical and chemical sputtering/erosion, material deposition and hydrogen/deuterium recycling. Less reliable data are known for electron emission from wall materials under impact of energetic ions, atoms and electrons [14, 15]. However, IEE plays an important role in PSI by influencing the boundary plasma (e.g. via the sheath potential) and consequently the intensity of plasma wall interaction. Basically, an extensive electron yield is expected to reduce the sheath potential. This in turn reduces the impact energy of ions and consequently the ion flux to the surface and the related sputtering yield. Therefore, the IEE data are needed as input for edge plasma modeling.

In this communication we describe a recently developed experimental setup and procedures for ion-induced electron yield measurements. Subsequently, we report preliminary results on electron yield measurements from carbon and aluminum targets bombarded with 1-10 keV singly charged ions $Ne^+$ and $Ar^+$.

## 2. Experimental Setup

The ion beam system has been described in detail elsewhere [16]. Briefly the ions were produced in an indigenously developed magnetically confined hollow cathode duoplasmatron [17] and extracted by biasing the extraction lens with 1-10 kV potential with respect to the ion source. The ion beam is then focused at the entrance aperture of $E \times B$ velocity filter by three electrodes Enzel lens. After charge and mass selection by $E \times B$ velocity filter, the ions were directed onto the 99.99% pure carbon or aluminum target that was placed inside a cage (see Fig. 1). The current density at the target surface was in the range of 2-10 $\mu A/cm^2$. The pressure in the target chamber was maintained at about $10^{-7}$ torr by differential pumping. The target was mechanically polished, ultrasonically cleaned and placed perpendicular to the ion-beam direction. In order to obtain the required clean surface, a self-sputtering process was performed using 10 keV $Ar^+$ ions. During the cleaning process the surface condition was checked by measuring at intervals the electron yield of the target. The electron yield decreases significantly upto a dose of $6\times10^{15}$ ions/cm$^2$ and then reaches a saturation value at about $3\times10^{16}$ ions/cm$^2$. The saturated electron yield indicates that oxide layers and adsorbed gases have been removed by ion sputtering. Additionally, during ion-induced photon emission studies it was observed that a clean target surface, having no characteristic emission from adsorbed gases, could be achieved after the dose of about $10^{16}$ ions/cm$^2$ [18]. All measurements reported in this work were performed after the electron yield from target has been saturated.

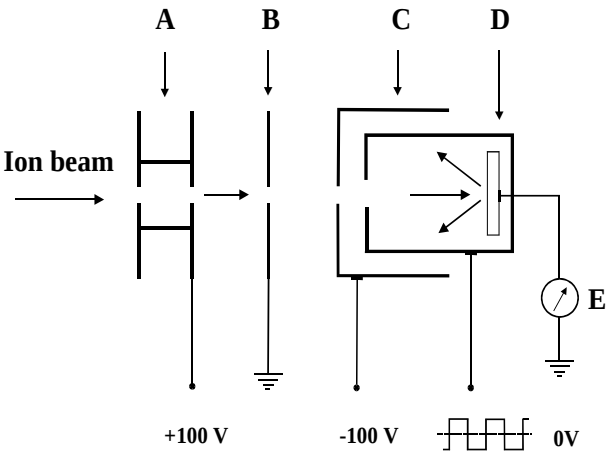


Figure 1. Schematic diagram of the experimental setup used for secondary electron emission studies. (A) Beam defining collimator, (B) Striping aperture, (C) rejection aperture, (D) cage and (E) Pico-ammeter.

Figure 1 shows schematics of the experiment setup used for secondary electron measurements. A beam defining collimator servers to prevent the incoming ions from directly impacting the forthcoming striping and rejection apertures and has a diameter of 2 mm. A potential of +100 V is applied to beam defining collimator to minimize ion-induced emission of electrons from its edges. The striping aperture prevents ions scattered by the collimator from entering the target region. The striping and rejection apertures have diameter of 3 mm and 3.5 mm respectively. A cage that is operated with a ± 80 V square wave generator surrounds the target in order to collect or suppress electrons emitted from the target. The cage has an aperture of 4.5 mm for ion beam entrance, through which the incident ion beam collimated to 2 mm in diameter is able to reach the target surface. A rejection electrode at a potential of –100V was placed before the cage that prevents electrons from escaping and thus further enhances the electron collection efficiency. The current at the target is measured with a pico-amper meter and then fed into a computer.

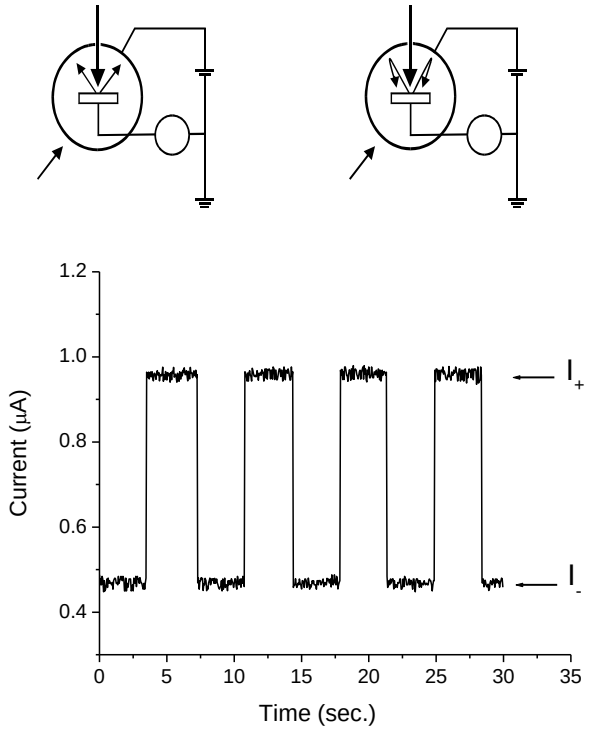


Figure 2. (a) Determination of total electron yields by measuring the currents $I_+$ and $I_-$. (b) Typical target current measured during 4 keV $Ne^+$ impact on the carbon for four consecutive bias pulses.

When applying + 80 V to the cage with respect to the target (see Fig. 2a), the total current $I_+$ that is measured at the target consists of two components, the currents of incoming ions $I_i$ and the current of emitted electrons $I_e$.

$$I_+ = I_i + I_e = I_i + \gamma(I_i/q) \quad (1)$$

Where $q$ is the charge of incoming ion. For – 80 V applied to the cage leads to a target current $I_-$ that is equal to the incoming ion current

$$I_- = I_i \quad (2)$$

Therefore, the total electron yield is given as [19]

$$\gamma = \frac{I_e}{(I_i/q)} = q\frac{I_+ - I_-}{I_-} \quad (3)$$

Typical target current (i.e. $I_+$ and $I_-$) measured during 4 keV $Ne^+$ impact on the carbon for four consecutive bias pulses are shown in Fig. 2b.

## 3. Results and Discussion

Total electron yields $\gamma$ measured for normal impact of $Ar^+$ and $Ne^+$ on carbon and aluminum targets are plotted versus ion energy in Fig. 3. The indicated errors include systematic errors from current measurements (± 4%), and possible influence of backscattered ions (± 1%). Sufficient cleanliness of the target surface and the reliability of our whole measurement using newly developed instrument have been assured by comparing results obtained for electron emission due to $Ar^+$ impact on aluminum with data from the literature [20] (see Fig. 3). Several trends can be deduced from the experimental results shown in Fig. 3: (1) For investigated ion-target combinations, $\gamma$ increases with ion energy in the range of 1-10 keV. However, for carbon increase of $\gamma$ is faster for $Ar^+$ impact as compared to the $Ne^+$, (2) $\gamma$ seems to have an impact energy threshold below 1 keV and (3) for $Ar^+$ impact electron emission from the carbon is consistently higher as compared to the aluminum.

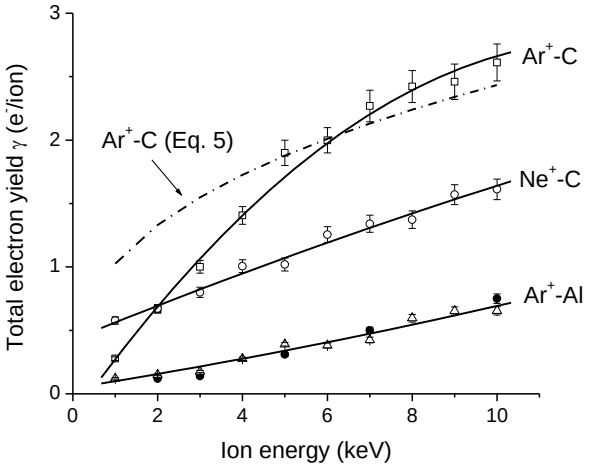


Figure 3. Total electron yields vs ion impact energy for various ion-target combinations: $Ar^+$-C (∀), $Ne^+$-C (–), $Ar^+$-Al (8). For $Ar^+$-Al combination data from Alonso et al. [20] is also shown (,). The solid lines through data points are drawn to guide the eye only. The broken line represents the calculated total electron yields using Eq. (5).

As mentioned in the introduction, total electron yield can result from a combination of Potential electron Emission (PE) and Kinetic electron Emission (KE). PE occurs mainly above and at the surface due to resonance and Auger transitions. Moreover, for PE a minimum ion potential energy of twice the surface work function is required [21],

but no threshold impact energy. The mechanism of PE is not very well explained by theories. According to the semi empirical formula given by Kishinevskii [22] potential electron emission yield can be expressed as

$$\gamma_{PE} \approx 0.2\left(0.8E_i - 2\phi\right)/\varepsilon \qquad (4)$$

where $E_i$ is the ionization energy of ions, $\varphi$ is the work function and $\varepsilon$ is the Fermi energy of target material. According to Eq. (4) $\gamma_{PE}$ from carbon upon impact of $Ar^+$ and $Ne^+$ is 0.074 and 0.204 $e^-$/ions respectively. In case of the projectile ion $Ne^+$, total electron emission yield below 2 keV impact energy is high as compared to $Ar^+$, which is most probably due to the important PE contributions in this low energy region. Now we will consider the KE contribution to the total electron yields. In almost all theories which are developed to explain the KE from surfaces [10], it is assumed that the mechanisms of the kinetic emission of electrons at low-energy ion impact consists of following three successive steps:

1. generation of electrons in solid by kinetic energy deposition from the incoming ions;
2. transport of these electrons towards the solid surface;
3. escape through the surface into vacuum.

It is therefore expected that above threshold the kinetic electron emission yield $\gamma_{KE}$ and the electronic stopping powers should have nearly the same dependence on the incident ion energy. Baragiola et al. [23] and Schou [24] had derived the following semi-empirical formula for $\gamma_{KE}$ for energetic ion impact

$$\gamma_{KE} = \frac{PL}{2J}\left(\frac{dE}{dX}\right)_e = \Lambda S_e \qquad (5)$$

where J is the mean energy for producing a free electron within solid, L is mean free path for electron in solid, P the mean escape probability by overcoming the surface barrier and $(dE/dX)_e = S_e$ the electronic stopping power of ions for solid. The impact energy dependence of $\gamma_{KE}$ derived from Eq. (5) are also plotted in Fig. 3, where electronic stopping power of $Ar^+$ ions for carbon target was calculated using TRIM code [25] and material parameter $\Lambda$ for carbon was taken equal to 0.01 nm/eV [10]. The electron yield measured from carbon upon impact of $Ar^+$ is in agreement with perditions of Eq. (5), especially above 5 keV impact energy.

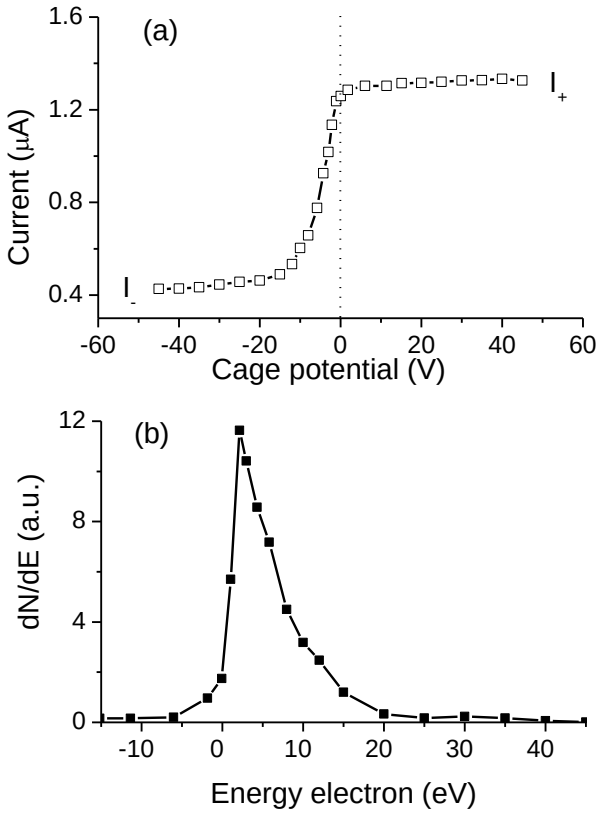


Figure 4. (a) Target current measured as a function of cage potential for impact of 5 keV $Ar^+$ ions on carbon, giving the integrated electron energy distribution *N(E)*. (b) Electron energy distribution *dN/dE* obtained from *N(E)*.

Although, dedicated analyzers (90º or 180º sectors) are designed to measure the energy of secondary electrons, it is possible to measure the energy distribution of secondary electrons in reasonably accurate way by operating the above described setup (Fig. 1) in retarding field configuration i.e. by varying the cage potential with respect to the target, while recording the target current. The target current measurements for varying cage potential (see Fig. 4a), resulted in integrated electron energy distribution *N(E)* for 5 keV $Ar^+$ impact on carbon. The electron energy distribution *dN/dE* derived from *N(E)* data by differentiation is shown in Fig. 4b. As it can be seen, the energy distribution of electrons has an intense peak at about 2.13 eV followed by monotonically decreasing tail, with the bulk of electrons having energies well below 20 eV. This

structure is comparable to previously reported energy distribution of electron ejected from various metals surfaces bombarded by $He^+$, $Ar^+$ and $Xe^+$ ion [2, 10]. The similarity of energy distribution of electrons released from various metal has been already reported by many investigators [9]. During the ion penetration of the solid, it is exposed to a series of collisions with target atoms, electron clouds of colliding partner interact with each other and as a result some electrons are promoted above the vacuum level. The electrons, which are librated during such a process, expected to have a continuous energy spectrum from nearly zero to a few tens of electron volts [26]. However, a number of additional structures on continuous energy spectrum have been recorded with special experimental arrangements [27, 28].

## 4. Conclusions

We have used a relatively simple experimental arrangement to measure total electron yield from carbon and aluminum targets upon impact of 1-10 keV ions of $Ar^+$ and $Ne^+$. The results obtained are in good agreement with the very modest amount of data available for comparison and also extend the parameter range previously reported in the literature thereby providing additional support for the theory. Our future work will concentrate to have a detailed and quantitative data on (1) potential and kinetic electron emission yields, (2) ion-energy thresholds for kinetic electron emission (3) dependence of the electron yields on mass and charge of ion as well as the target temperature. Furthermore, the majority of measurements of electron emission yields reported in the literature were performed with atomic ions and little is known about electron emission by molecular and cluster ions. It will be interesting to investigate whether for ions of same velocity the electron emission yield scale like the number of atoms of projectile molecular ion.

## Acknowledgement

The authors are indebted to several technicians of General Service Division PINSTECH for construction of the apparatus and M. Ashraf and M.K. Hayat for assistance during measurements.

## References

[1] R.A. Baragiola, Nucl. Instr. Meth. B **78** (1993) 223.

[2] N. Benazeth, Nucl. Instr. Meth. **194** (1982) 405.

[3] H.D. Hagstrum, Phys. Rev. **96** (1954) 336.

[4] P. Sigmund and S. Tougaard, in Inelastic Particle Surface Collisions, edited by E. Taglauer and W. Heiland, Springer Series in Chemical Physics Vol. 17 (Springer-verlag, Berlin 1981), p.2.

[5] M. Delaunay, M. Fehringer, R. Geller, D. Hitz, P. Varga and H. Winter, Phys. Rev. B**35** (1987) 4232.

[6] E.J. Sternglass, Phys. Rev. **108** (1957) 1.

[7] J. Schou, Scanning Electron Microsc. **2** (1988) 607.

[8] O. Benka, E. Steinbauer and P. Bauer, Nucl. Instr. Meth. B **90** (1994) 64.

[9] M. Rosler and W. Braue, in Particle Induced Electron Emission I, Eds G. Hohler, Vol. 122, (Springer, Berlin 1991).

[10] D. Hasselkamp, in Particle Induced Electron Emission II, edited by G. Hohler, Vol. 123, Springer, Heidelberg, 1992.

[11] W. O. Hofer and J. Roth, Physical Processes of the interaction of fusion plasmas with solids (Academic Press, San Diego, 1996).

[12] R.K. Janev, Eds., Atomic and Molecular Processes in Fusion Edge Plasma, (Plenum, New York, 1995).

[13] P. C. Stangeby and G. M. McCracken, Nucl. Fusion **30** (1990) 1225.

[14] A. Qayyum, W. Schustereder, C. Mair, P. Scheier, T. D. Märk, S. Cernusca, HP. Winter and Aumayr, J. Nucl. Mat. **313** (2003) 670.

[15] E. W. Thomas, Atomic Data for Controlled Fusion Research (ORNL, 1985).

[16] A. Qayyum and M.N. Akhtar, Eur. Phys. J. D **12** (2000) 181.

[17] A. Qayyum and S. Ahmad, Nucl. Instr. and Meth. B **94** (1994) 597.

[18] A. Qayyum, M.N. Akhtar and T. Riffat, Radiat. Phys. Chem. **72** (2005) 663.

[19] H. Eder, W. Messerschmidt, H.P. Winter and F. Aumayr, J. Appl. Phys., **87** (2000) 8198.

[20] E.A. Alonso, R.A. Baragiola, J. Ferron, M.M. Jakas and A. Oliva-Florio, Phys. Rev. B **22** (1980) 80.

[21] H.D. Hagstrum, Phys. Rev. **96** (1954) 336.

[22] L.M. Kishinevkii, Radiat. Eff. **19** (1973) 23.

[23] R.A. Baragiola, E.A. Alonso, J. Ferron and A. Oliva, Sur. Sci. **90** (1979) 240.

[24] J. Schou, Phys. Rev. B **22** (1980) 2141.

[25] J.F. Ziegler, J.P. Biersack, U. Littmark, The stopping and range of ions in solids, (Pergamon Press, New York, 1985).

[26] W. Soszka, Nucl. Instr. Meth. B **61** (1991) 547.

[27] W. Soszka, Nucl. Instr. Meth. B **78** (1993) 260.

[28] H. Rothard, M. Schosnig, K. Kroneberger and K. Groeneveld, Phys. Rev. B **46** (1992) 11847.